# Selective aerobic oxidation reactions using a combination of photocatalytic water oxidation and enzymatic oxyfunctionalizations

Zhang, Wuyuan; Fernández-Fueyo, Elena; Ni, Yan; Van Schie, Morten; Gacs, Jenö; Renirie, Rokus; Wever, Ron; Mutti, Francesco G.; Rother, Dörte; Alcalde, Miguel

**DOI**
10.1038/s41929-017-0001-5

**Publication date**
2018

**Document Version**
Final published version

**Published in**
Nature Catalysis

nature catalysis

ARTICLES

https://doi.org/10.1038/s41929-017-0001-5

# Selective aerobic oxidation reactions using a combination of photocatalytic water oxidation and enzymatic oxyfunctionalizations

Wuyuan Zhang[1], Elena Fernández-Fueyo[1], Yan Ni[1], Morten van Schie[1], Jenö Gacs[1], Rokus Renirie[2], Ron Wever[2], Francesco G. Mutti[2], Dörte Rother[3], Miguel Alcalde[4] and Frank Hollmann[1]*

**Peroxygenases offer an attractive means to address challenges in selective oxyfunctionalization chemistry. Despite this, their application in synthetic chemistry remains challenging due to their facile inactivation by the stoichiometric oxidant $H_2O_2$. Often atom-inefficient peroxide generation systems are required, which show little potential for large-scale implementation. Here, we show that visible-light-driven, catalytic water oxidation can be used for in situ generation of $H_2O_2$ from water, rendering the peroxygenase catalytically active. In this way, the stereoselective oxyfunctionalization of hydrocarbons can be achieved by simply using the catalytic system, water and visible light.**

Selective oxyfunctionalization of carbon–hydrogen bonds is still an unachieved dream reaction in organic synthesis[1–3]. In particular, balancing the reactivity of the oxygen-transfer reagent with selectivity is largely unsolved for (in)organic catalysts, while it is an inherent feature of many oxidative enzymes such as haem-dependent monooxygenases and peroxygenases. The relevance of peroxygenases (UPO, unspecific peroxygenase; IUBMB classification: EC 1.11.2.1) for selective oxyfunctionalization reactions in preparative organic synthesis is increasing rapidly[4], especially the novel peroxygenases from *Agrocybe aegerita* (*Aae*UPO)[5], *Marasmius rotula* (*Mro*UPO)[6] and *Coprinopsis cinerea* (*Cci*UPO)[7], which excel in terms of substrate scope and specific activity compared with the well-known chloroperoxidase from *Caldariomyces fumago* (*Cfu*UPO)[8], P450 monooxygenases and chemical counterparts. The very high turnover numbers (TONs) reported so far give reason to expect truly preparative-scale applications for these promising biocatalysts. Additionally, crystal structures of *Aae*UPO[9] as well as directed evolution protocols[10] together with efficient recombinant expression systems have been established in the past few years. Hence, current gaps in substrate scope, stability and/or selectivity will be closed[1,11–13].

In contrast to P450 monooxygenases, peroxygenases do not rely on complicated and susceptible electron transport chains delivering reducing equivalents to the haem active site needed for reductive activation of molecular oxygen and therefore are not subject to the 'oxygen dilemma'[14]. Rather, peroxygenases utilize $H_2O_2$ directly to regenerate the catalytically active oxyferryl haem species. At the same time, however, peroxygenases suffer (like all haem-dependent enzymes) from a pronounced instability against $H_2O_2$, making controlled in situ provision of $H_2O_2$ inevitable. Today, the well-known glucose/glucose oxidase system to generate $H_2O_2$ from $O_2$ prevails on the lab-scale, but shows little potential for larger, preparative applications due to its poor atom-efficiency[15]. More efficient electron donors such as small alcohols or electrochemical sources have recently been proposed[16,17].

Ideally, water could serve as a co-substrate and electron donor for the in situ generation of $H_2O_2$. Peroxygenase reactions are generally conducted in aqueous media ($[H_2O] = 55$ mol $l^{-1}$) and the sole by-product of the water oxidation reaction is molecular oxygen. A broad variety of heterogeneous water oxidation catalysts (WOCs) have been reported in recent years that could be used for the partial oxidation of water to hydrogen peroxide[18,19]. The thermodynamic driving force for this reaction is derived from (visible) light. This approach is mostly evaluated with respect to catalytic water splitting into $H_2$ and $O_2$. However, under aerobic conditions, electrons liberated from water can also be transferred to $O_2$ yielding $H_2O_2$; incomplete oxidation of water to $H_2O_2$ can also be conceived.

This motivated us to evaluate photochemical water oxidation yielding $H_2O_2$ to promote peroxygenase-catalysed, selective oxyfunctionalization reactions (Fig. 1). Here, we demonstrate the general feasibility of this approach together with a characterization of the crucial parameters determining activity and robustness of the reaction scheme. The selective, photoenzymatic oxyfunctionalization of a range of hydrocarbons is demonstrated, as is the embedding of this reaction scheme into more-extended cascades producing value-added chiral alcohols and amines.

## Results

**Proof-of-concept experiments.** As our model enzyme we chose the UPO from *A. aegerita*, which was recombinantly expressed in *Pichia pastoris* (r*Aae*UPO) following a previously reported protocol[20]. The enzyme was purified to near homogeneity by a single anion exchange chromatography step (Supplementary Figs. 5 and 6). The enzyme preparation used herein exhibited a Reinheitszahl (Rz: $A_{420}/A_{280}$) value of 1.6. As our model reaction we chose the stereoselective hydroxylation of ethyl benzene to (*R*)-1-phenyl ethanol (Fig. 2). Visible-light-active Au-loaded $TiO_2$ was used as photocatalyst for the proof-of-concept experiments[21].

Under arbitrarily chosen reaction conditions (Fig. 2) we observed significant accumulation of (*R*)-1-phenyl ethanol as

[1]Department of Biotechnology, Delft University of Technology, Delft, The Netherlands. [2]Van't Hoff Institute for Molecular Sciences (HIMS), Faculty of Science, University of Amsterdam, Amsterdam, The Netherlands. [3]Institute of Bio- and Geosciences, IBG-1: Biotechnology, Forschungszentrum Jülich GmbH, Jülich, Germany. [4]Department of Biocatalysis, Institute of Catalysis, CSIC, Madrid, Spain. *e-mail: f.hollmann@tudelft.nl

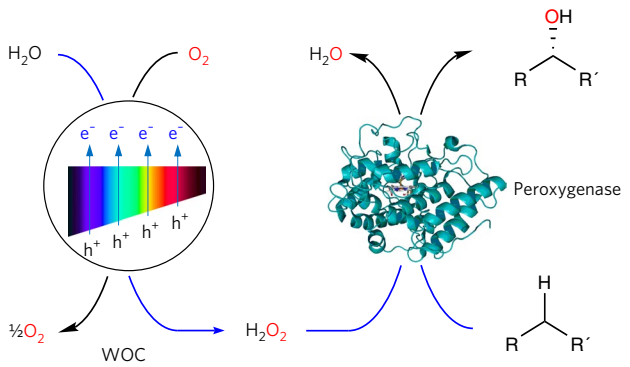


**Fig. 1 | Photochemical water oxidation generating $H_2O_2$ to promote peroxygenase-catalysed hydroxylations.** A water oxidation catalyst (WOC) mediates the photochemical oxidation of water and delivers the liberated reducing equivalents to molecular oxygen to produce $H_2O_2$. The latter is utilized by a peroxygenase to catalyse (stereo)selective oxyfunctionalization reactions.

desired. Control reactions in the absence of the Au-$TiO_2$ photocatalyst or in darkness yielded no product. The absence of the enzyme or using a thermally inactivated enzyme resulted in a slow accumulation of racemic 1-phenyl ethanol (less than 0.14 mM within 24 h) and approximately the same concentrations of acetophenone. This minor background oxidation activity of the photocatalyst explains the slightly decreased optical purity of the (*R*)-1-phenyl ethanol obtained from the photobiocatalytic oxidation reactions (90% e.e.) as compared with traditional reaction schemes for the provision of r*Aae*UPO with $H_2O_2$ (>97% e.e.)[22].

Particular attention was paid to the nature of the electron donor for this reaction as, in principle, other reaction components may also be susceptible to $TiO_2$ oxidation and thereby serve as sacrificial electron donors for the reduction of $O_2$. For this, the enzyme preparation contained phosphate only as a buffer component to exclude possible contributions of other sacrificial electron donors to $H_2O_2$ generation. Experiments using immobilized enzymes were also conducted to exclude r*Aae*UPO oxidation to promote $H_2O_2$ generation. To further support the assumed water-oxidation-based mechanism, we performed a range of experiments using $^{18}O$-labelled water as the reaction mixture. The occurrence of $^{18}O$-labelled (*R*)-1-phenyl ethanol (Supplementary Fig. 10) substantiates the proposed mechanism. Performing this experiment in the presence of ambient air (predominantly consisting of $^{16}O_2$) resulted in minor incorporation of $^{18}O$ into the product, which predominantly contained $^{16}O$. Using deaerated reaction mixtures (wherein only water oxidation can account for $O_2$), the $^{18}O$-labelled product dominated. These findings strongly support the suggested $TiO_2$-mediated oxidation of $H_2O$ to $O_2$ coupled to $TiO_2$-catalysed reduction of $O_2$ to $H_2O_2$, which is used by r*Aae*UPO for specific incorporation into ethyl benzene. A contribution of $H_2O_2$ originating from direct two-electron water oxidation is also possible[23]. These results make us confident that water indeed served as the sole source of reducing equivalents to promote the selective r*Aae*UPO-catalysed oxyfunctionalization reactions.

**Characterization of the photoenzymatic oxyfunctionalization reaction.** Next, we advanced to characterize the reaction system in more detail, particularly investigating the effect of varying catalyst concentrations on the reaction system. It is worth mentioning here that the product concentrations shown in Fig. 2 may appear low, but they significantly surpass the concentrations of $H_2O_2$ obtained from water oxidation reported so far for Au-$TiO_2$ and other WOCs[19,24]. We attribute this to a $H_2O_2$-oxidation activity of the illuminated WOCs (Supplementary Fig. 11) eventually leading to a low steady-state concentration of $H_2O_2$ (ref. [25]). At first sight, this may appear as a limitation for the current system, but it also enables us to maintain low, constant in situ concentrations of $H_2O_2$ as required for efficient and robust peroxygenase catalysis.

The concentration of the WOC had only a minor influence on the initial rate of the reaction (Fig. 2b). We attribute this to WOC-concentration-independent in situ $H_2O_2$ concentrations, most probably due to the simultaneous water- and $H_2O_2$-oxidation activity of the WOCs mentioned above. The WOC concentration, however, had a very significant influence on the robustness of the overall reaction. In general, no more product accumulation was observable after approximately 6 h. Varying the Au content (0.6–1.8 wt%) and particle size (2.8–7.9 nm) on the $TiO_2$ surface hardly influenced the time course of the photobiocatalytic hydroxylation reaction, with the exception of plain $TiO_2$ where the overall rate was approximately half of the rates obtained with various Au-$TiO_2$ catalysts (Supplementary Fig. 12).

In contrast, the enzyme concentration directly influenced the overall reaction rate (Fig. 2c) and a linear dependency of initial (*R*)-1-phenyl ethanol accumulation on applied r*Aae*UPO concentration was observed. However, again, the reactions ceased after 6–7 h.

Apparently, the robustness of the overall reaction (as judged from the accumulation of (*R*)-1-phenyl ethanol) correlated with the ratio of photo- and bio-catalyst. We hypothesized that r*Aae*UPO may be inactivated by the Au-$TiO_2$ WOC. It should be mentioned here that in the experiments reported so far, only $TiO_2$ mostly composed of anatase phase (91.1%) had been used as the WOC. Given the rather hydrophilic surface of anatase $TiO_2$, adsorption of the glycoprotein r*Aae*UPO appears likely. Therefore, we performed control experiments to investigate the inactivation of the biocatalyst: incubation of the enzyme with the photocatalyst in darkness resulted in a minor reduction of its catalytic activity as compared to the same experiment in the presence of light (Fig. 3). Therefore, we conclude that it is not the adsorption per se that leads to inactivation of the biocatalyst.

We hypothesized that reactive oxygen species (ROS) generated at the surface of the WOC[26] may cause oxidative inactivation of the enzyme. In fact, using the spin trap technique in electron paramagnetic resonance (EPR) spectroscopy, significant amounts of mainly hydroxyl ($HO^{\bullet}$) radicals (spin Hamiltonian parameter of hydrogen nucleus $a_H = 1.495$ mT; constant of proportionality factor $g = 2.0050$) could be detected in illuminated anatase-Au-$TiO_2$ samples (Fig. 4a)[26]. These hydroxyl radicals may originate from water oxidation, from the reaction of superoxide ($O_2^{\bullet-}$, from $O_2$ reduction) or from other steps in the complex redox chemistry of ROS[27]. Though more detailed mechanistic studies will be necessary to fully understand this inactivation mechanism, we hypothesize a major role of hydroxyl rather than the superoxide radicals. First, addition of superoxide dismutase did not improve the robustness of the overall reaction. Second, $O_2^{\bullet-}$ should react with native peroxygenase leading to the formation of the so-called Compound III of the catalytic cycle, for which we have not found any spectroscopic evidence (no characteristic absorption peak at 625 nm, Supplementary Fig. 14)[28].

**Overcoming robustness issues through separation.** Given the rather short half-life time of hydroxyl radicals (approximately $10^{-9}$ s in aqueous media) we envisioned that simple spatial separation of the WOC (at the surface of which the $HO^{\bullet}$ radicals form) and the biocatalyst may circumvent this limitation. Therefore, we evaluated (1) spatial separation of anatase Au-$TiO_2$ from r*Aae*UPO using immobilized enzymes and (2) avoidance of r*Aae*UPO adsorption to the WOC surface by using hydrophobic surfaces.

To achieve physical separation of the WOC and r*Aae*UPO, we covalently immobilized the latter to a poly(methyl methacrylate) resin activated by glutardialdehyde. Covalent linkage to the spacer unit occurred through imine formation with surface-exposed lysine

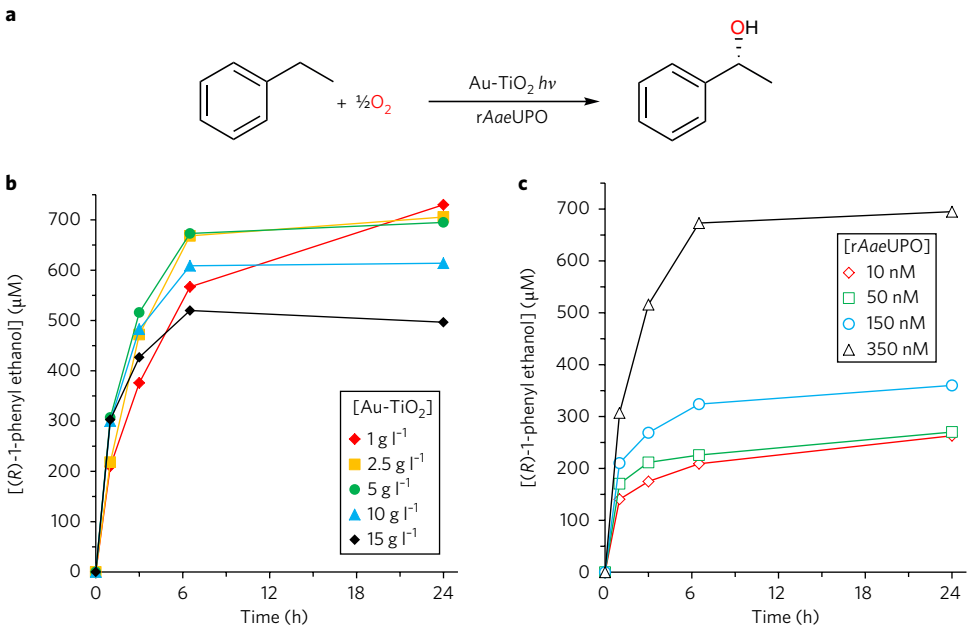


**Fig. 2 | Time courses of the photoenzymatic hydroxylation of ethyl benzene at varying catalyst concentrations. a**, Reaction scheme. General conditions: reactions were performed in 60 mM phosphate buffer (pH 7.0) under visible light illumination ($\lambda > 400$ nm), $T = 30$ °C, [ethyl benzene] = 15 mM. **b**, [r*Aae*UPO] = 350 nM, [Au-$TiO_2$] = 1–15 g $l^{-1}$. **c**, [Au-$TiO_2$] = 5 g $l^{-1}$, [r*Aae*UPO] = 10–350 nM.

residues (Supplementary Fig. 7). To test the second option, that is, avoidance of enzyme adsorption by less hydrophilic WOC surfaces, rutile Au-$TiO_2$ was evaluated. Rutile exhibits a far more hydrophobic surface as compared with the previously used anatase catalyst. This is corroborated by the lack of the characteristic IR absorptions of surface-bound $H_2O$ and Ti-OH (even after Au-doping treatment) at 3,422 and 1,632 $cm^{-1}$, respectively (Supplementary Fig. 13). This leads to the assumption that the heavily glycosylated r*Aae*UPO may be less prone to adsorption to rutile than to anatase surfaces. Hence, while the photoelectrochemical properties (that is, the redox potential and energy levels of conducting and valence bands)[30] of both crystal phases are comparable, rutile should be preferable due to its expected lower adsorption tendency for proteins. Indeed, r*Aae*UPO adsorbed approximately 10 times less to rutile as compared with anatase catalyst (Supplementary Figs. 15 and 16). Furthermore, this effect does not appear to be limited to glycoproteins such as r*Aae*UPO as a bacterial enzyme (the old yellow enzyme homologue from *Bacillus subtilis*, YqjM)[31] also showed similar adsorption behaviour to r*Aae*UPO (Supplementary Fig. 17). Overall, both strategies appeared suitable to minimize oxidative inactivation of r*Aae*UPO at the photocatalyst surface and therefore should lead to more robust photobiocatalytic hydroxylation reactions. Figure 5 compares the time courses of these catalytic systems.

In both cases, steady product accumulation was observed for at least 120 h, thereby representing a >20-fold increase in robustness as compared with the starting conditions (Fig. 5). Consequently, the TON of the enzyme increased from approximately 2,000 using dissolved enzyme and anatase Au-$TiO_2$ to more than 16,000 using immobilized r*Aae*UPO and 21,000 using rutile Au-$TiO_2$ (Fig. 5). The latter system also provided (*R*)-1-phenyl ethanol in much higher optical purity (>98% e.e.) compared with the starting conditions. The reaction using immobilized r*Aae*UPO was considerably slower than the reaction using free r*Aae*UPO and rutile Au-$TiO_2$. This may, at least to some extent, be attributed to diffusion limitations originating from the doubly heterogeneous character of the catalysts. Also, partial loss of enzyme activity as a consequence of the immobilization may contribute to this[32]. To clarify this, systematic immobilization studies with r*Aae*UPO are currently ongoing.

The turnover frequency of r*Aae*UPO of 2.9 $min^{-1}$ (average over 4 days) indicates that there is room for improving the efficiency of this reaction system. Indeed, increasing the rutile Au-$TiO_2$ concentration linearly increased the initial rate of the overall reaction (Supplementary Fig. 18). Surprisingly, an EPR investigation of the rutile-Au-$TiO_2$ catalysed water oxidation (Fig. 4b) revealed that this catalyst generates significantly higher amounts of HO• radicals than anatase Au-$TiO_2$. In fact, as already stated, a higher amount of superoxide may be formed by rutile Au-$TiO_2$. At first sight this is in contrast to the higher compatibility of rutile Au-$TiO_2$ with the enzymes investigated. It may, however, be rationalized by the poor

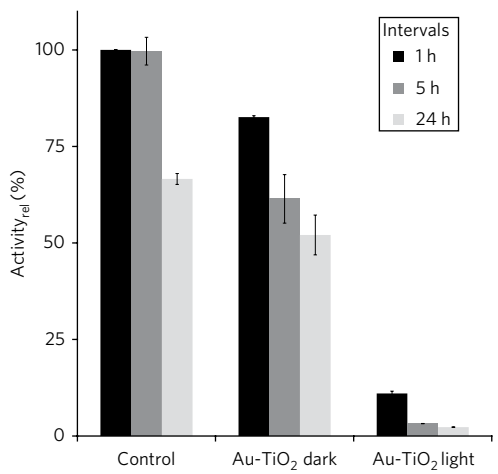


**Fig. 3 | Stability of r*Aae*UPO in the presence of anatase-Au-$TiO_2$.** General conditions: phosphate buffer (60 mM, pH 7.0), $T = 30$ °C, [anatase-Au-$TiO_2$] = 0 (control, under illumination) or 10 g $l^{-1}$, [r*Aae*UPO] = 150 nM. The samples were either kept in darkness or illuminated under visible light ($\lambda > 400$ nm). Samples were withdrawn at intervals (shades of grey) from the incubation mixtures and analysed for peroxygenase activity. Error bars indicate the standard deviation of duplicate experiments ($n = 2$).

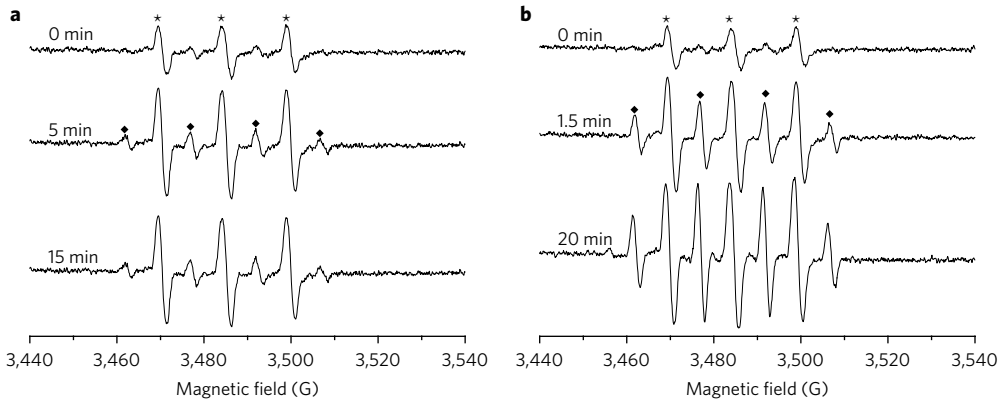


**Fig. 4 | EPR spectra recorded during the illumination of anatase and rutile Au-$TiO_2$ in water. a**, Anatase Au-$TiO_2$. **b**, Rutile Au-$TiO_2$. Signals marked by asterisks belong to the existing oxidation product of DMPO, 5,5-dimethyl-2-oxopyrroline-1-oxyl (DMPOX);[29] signals marked with solid diamonds belong to the spin-adduct DMPO-OH•, which are not overlapping the signals of DMPOX and therefore provide sufficient quality for analysis. Reaction conditions: [Au-$TiO_2$] = 5.0 mg $ml^{-1}$, [DMPO] = 30 mM, RT, $h\nu$ > 400 nm. DMPO, 5,5-dimethyl-1-pyrroline *N*-oxide.

adsorption tendency of proteins to the rutile-$TiO_2$ surface and the very short half-life of the hydroxyl radical resulting in very short diffusion distances[33].

**Substrate scope of the photoenzymatic reaction.** Encouraged by these results, we further explored the product scope of the photoenzymatic hydroxylation reaction using dissolved r*Aae*UPO and rutile Au-$TiO_2$. As shown in Table 1, a broad range of aliphatic and aromatic compounds were converted into their corresponding alcohols. The enantioselectivities and relative activities corresponded to the values reported previously, indicating that the natural reactivity and selectivity of the enzyme were not impaired[34,35]. Similar results were also observed in the system utilizing anatase Au-$TiO_2$ and immobilized enzyme (Supplementary Table 2). Semipreparative-scale reactions also proved to be feasible with this setup (Supplementary Figs. 28–30). Hence, approximately 110 mg of highly enantioenriched (e.e. = 97.4%, 31% isolated yield) (*R*)-1-phenyl ethanol was produced.

The regioselectivity of all reactions was very high except for entry 7 where ω-2 and ω-3 hydroxylation products were observed. This observation is in line with previous reports on r*Aae*UPO-selectivity towards linear alkanes[36].

**Cascade reactions.** Generally, the only by-product observed was the 'overoxidation' product, that is, the corresponding ketone. We suspected WOC-catalysed further oxidation of the primary r*Aae*UPO-product ((*R*)-1-phenyl ethanol) accounted for this. Indeed, the concentration of acetophenone linearly increased with increasing concentrations of Au-$TiO_2$ (Supplementary Table 3). This dual activity of the photocatalyst (water and alcohol oxidations) motivated us to evaluate more elaborate photoenzymatic cascades to extend the product scope beyond (chiral) alcohols. In particular, we coupled the photoenzymatic oxidation of toluene to benzaldehyde to an enzymatic benzoin condensation using the benzaldehyde lyase from *Pseudomonas fluorescens* (*Pf*BAL) (Fig. 6a)[37,38]. Acetophenone, formed by the photoenzymatic oxyfunctionalization of ethyl benzene, was also submitted to a reductive amination using the ω-transaminases from *Aspergillus terreus* (*R*-selective, *At*ωTA) and *Bacillus megaterium* (*S*-selective, *Bm*ωTA) (Fig. 6b)[39,40]. Both cascades were performed in a one-pot two-step fashion, that is, the photoenzymatic oxidation to the corresponding aldehyde or ketone was performed first, followed by addition of the biocatalysts needed for the second transformation (Supplementary Figs. 31–35). Recently, a similar transformation was reported (ethyl benzene to enantiomerically pure (*R*)- or (*S*)-1-phenyl ethyl amine) attaining very similar product titers[41]. It is worth mentioning that a one-pot one-step procedure was also possible in the case of the second cascade (Fig. 6b), albeit at somewhat lower product yields (0.7 mM, 37% e.e. and 0.5 mM, 99% e.e. for (*R*)- and (*S*)-1-phenyl ethyl amine, respectively).

These results demonstrate that the proposed photoenzymatic cascades enable synthesis of a broader range of value-added products (chiral alcohols, amines and acyloins) from simple starting materials. While these reactions undoubtedly still need further improvement to reach preparative feasibility, they nevertheless demonstrate the principal feasibility of the envisioned photoenzymatic cascade reactions.

The proposed in situ $H_2O_2$ generation system can also be applied to other peroxidases such as the V-dependent haloperoxidase from

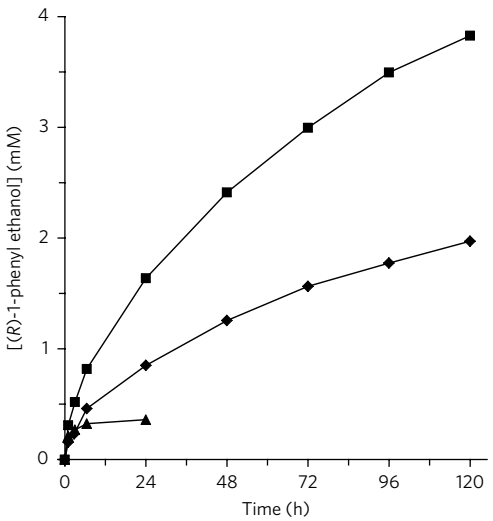


**Fig. 5 | Effect of reducing the interaction of r*Aae*UPO with the $TiO_2$ surface on the robustness of the photoenzymatic reaction.** Original reaction setup with dissolved r*Aae*UPO and anatase Au-$TiO_2$ (triangles); reaction using immobilized r*Aae*UPO and anatase Au-$TiO_2$ (diamonds); dissolved r*Aae*UPO with hydrophobic rutile Au-$TiO_2$ (squares). General conditions: [r*Aae*UPO] = 150 nM (dissolved), 120 nM (immobilized); [Au-$TiO_2$] = 5 g $l^{-1}$, $[\text{ethyl benzene}]_0$ = 15 mM ethyl benzene in 60 mM phosphate buffer (pH 7.0) under visible light illumination ($\lambda$ > 400 nm).

**Table 1 | Substrate scope of the photobiocatalytic hydroxylation reaction**

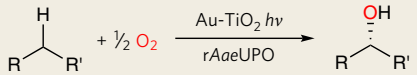


| Entry[a] | Product | Concentration (mM) | e.e. (%) | Other products | Concentration (mM) | Yield (%)[b] | TON (×10³)[b] |
|---|---|---|---|---|---|---|---|
| 1 |  | 4.1 | N/A |  | 0.5 | 45.2 | 30.1 |
| 2 | 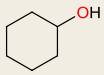 | 4.2 | N/A |  | 0.1 | 43.1 | 28.7 |
| 3 | 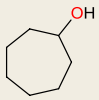 | 2.6 | N/A |  | 0.1 | 26.7 | 17.8 |
| 4 | 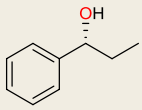 | 2.3 | >99.0 | 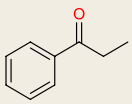 | 0.5 | 28.2 | 18.8 |
| 5 | 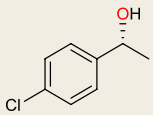 | 3.6 | 95.2 | 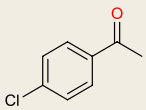 | 1.0 | 45.8 | 30.5 |
| 6 | 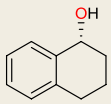 | 5.0 | 75.0 | 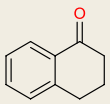 | 0.8 | 58.2 | 38.8 |
| 7 | 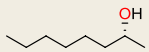 | 0.3 | 78.5 | 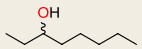 | 0.2 | 4.8 | 3.2 |

[a]Conditions: $[substrate]_0$ = 10.0 mM; [rutile Au-$TiO_2$] = 10 g $l^{-1}$; [r*Aae*UPO] = 150 nM (dissolved) in phosphate buffer (pH 7.0, 60 mM), $T$ = 30 °C, 70 h, visible light illumination ($\lambda$ > 400 nm).[b]Based on the concentration of both products. N/A, not applicable.

*Curvularia inaequalis* (*Ci*VCPO)[42,43]. Gratifyingly, the *Ci*VCPO-catalysed halogenation of thymol proceeded smoothly yielding 2- and 4-bromothymol with more than 70% conversion (Fig. 7). The product distribution was comparable to previous haloperoxidase-catalysed halogenation reactions[44,45]. In the absence of either *Ci*VCPO, rutile Au-$TiO_2$ or light, no conversion of thymol was observed. It is also worth mentioning that rutile Au-$TiO_2$ with this enzyme gave better results than anatase Au-$TiO_2$ under otherwise identical conditions.

**Beyond $TiO_2$-based WOCs.** So far, we have focused on $TiO_2$-based photocatalysts. Photocatalysis, however, is an extremely dynamic

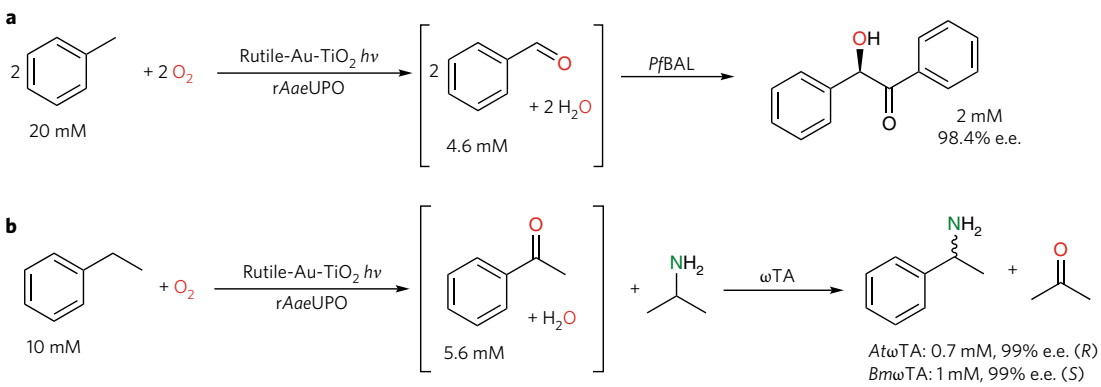


**Fig. 6 | Photoenzymatic cascade reactions. a**,**b**, The transformation of toluene to (*R*)-benzoin (**a**) and the transformation of ethyl benzene to (*R*)- or (*S*)-1-phenyl ethyl amine (**b**). Conditions for **a**: [toluene] = 20.0 mM, [rutile Au-$TiO_2$] = 30 g $l^{-1}$, [r*Aae*UPO] = 150 nM in phosphate buffer (pH 7.0, 60 mM), $T$ = 30 °C, 96 h, visible light illumination ($\lambda$ > 400 nm). In the second step, 100 μl of mixture in phosphate buffer (500 mM, pH 8.5) containing 5 mM of thiaminpyrophosphate (TPP), 25 mM of $MgCl_2$ and 10 mg of crude cell extract containing *Pf*BAL was added. Conditions for **b**: [ethyl benzene] = 10.0 mM, [rutile Au-$TiO_2$] = 30 g $l^{-1}$, [r*Aae*UPO] = 150 nM in phosphate buffer (pH 7.0, 60 mM), $T$ = 30 °C, 96 h. In the second step, 105 μl of isopropylamine, 130 μl of phosphoric acid (5 M), 100 μl of pyridoxal phosphate (PLP, 10 mM) and 10 mg of crude cell extract containing ω-transaminase were added. The pH of the mixture was adjusted to approximately 9.0. The dilution factor of the reaction system was 1.0/1.335 = 0.75. After the first steps under illumination and initiation of the second steps, the resulting reaction mixture of both cascades was shaken at 30 °C for 40 h in the dark.

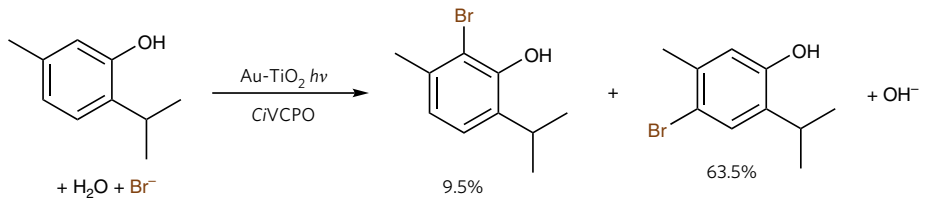


**Fig. 7 | Photoenzymatic halogenation of thymol.** Conditions: [rutile Au-$TiO_2$] = 5 g $l^{-1}$, [*Ci*VCPO] = 150 nM, [thymol] = 3 mM, [KBr] = 6 mM, [$Na_3VO_4$] = 50 μM in 1.0 ml citrate buffer (50 mM, pH 5.0), $T$ = 30 °C, $t$ = 70 h. The reaction mixture was irradiated by visible light ($\lambda$ > 400 nm).

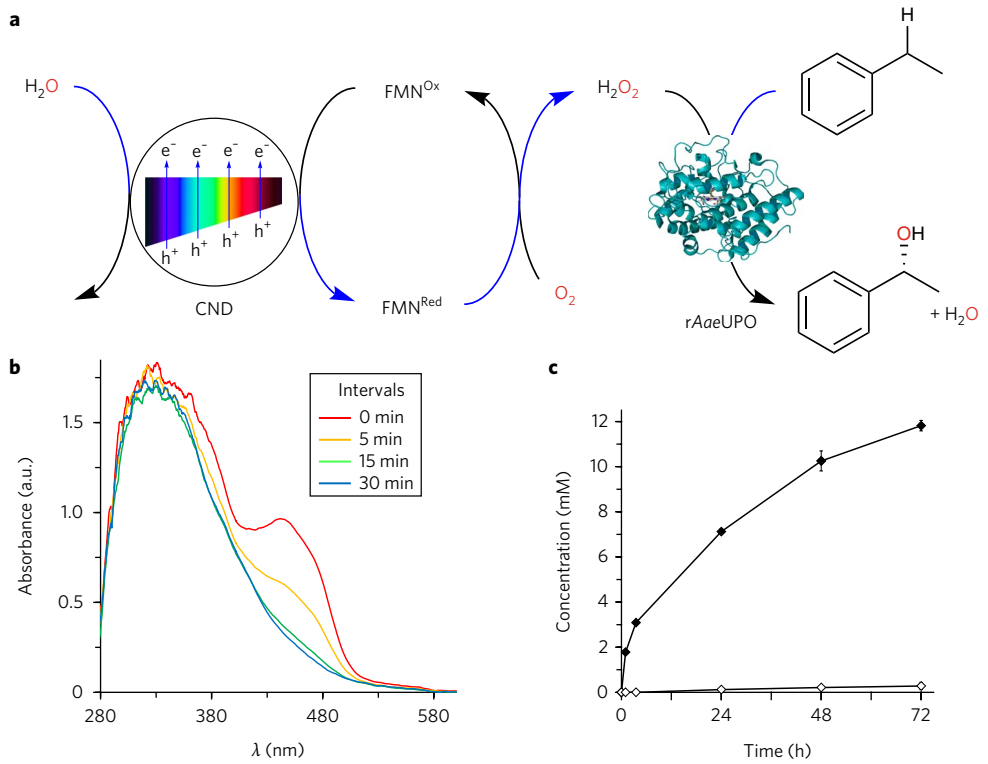


**Fig. 8 | Photoenzymatic reactions using CND photocatalysts and FMN cocatalysts. a**, Proposed reaction scheme. **b**,**c**, UV-spectroscopic investigation of the photocatalytic reduction of FMN (**b**) and example time course of the complete reaction system (**c**). General conditions for **b**: reaction was performed under anaerobic conditions in a glove box. Reaction conditions: [CND] = 1 g $l^{-1}$ and [FMN] = 0.05 mM in phosphate buffer pH 7.0 (60 mM), $\lambda$ = 450 nm, at intervals of 0–30 min the reaction mixtures were analysed by UV–vis spectroscopy. Reaction conditions for **c**: [r*Aae*UPO] = 120 nM, [ethyl benzene] = 15 mM, [CD] = 5 g $l^{-1}$ and [FMN] = 0.1 mM (filled diamonds) or 0 mM (open diamonds) in 60 mM phosphate buffer (pH 7.0) under visible light irradiation ($\lambda$ > 400 nm). Error bars indicate the standard deviation of duplicate experiments ($n$ = 2).

area of research and novel, potentially useful WOCs are reported on an almost weekly basis. Therefore, we finally evaluated the scope of different WOCs for the in situ generation of $H_2O_2$ to promote peroxygenase-catalysed hydroxylation reactions. Among them, visible-light-active Au-$BiVO_4$ (ref. [19]) and g-$C_3N_4$ (ref. [46]) showed some promising characteristics (Supplementary Fig. 36). The product formation with Au-$BiVO_4$ as photocatalyst was rather modest, while g-$C_3N_4$ exhibited a higher product formation rate together with a pronounced 'overoxidation activity' (approximately 10 times higher than Au-$TiO_2$ under comparable conditions)[47]. Therefore, the latter catalyst may be particularly suitable for further photobiocatalytic cascades.

Finally, recently described carbon nanodot (CND) photocatalysts caught our attention as easy-to-prepare and biocompatible photocatalysts[48–50]. As CND-mediated reduction of molecular oxygen to $H_2O_2$ is impaired[48], we used riboflavin monophosphate (flavin mononucleotide, FMN) as co-catalyst for the generation of $H_2O_2$ (Fig. 8). Visible-light illumination of a mixture of CND and FMN in deaerated phosphate buffer resulted in fast and complete reduction of FMN, as judged by the decrease of the characteristic absorption band of $FMN^{Ox}$ at 450 nm (Fig. 8b). Exposure to ambient atmosphere resulted in complete restoration of this absorbance, indicating aerobic reoxidation of $FMN^{Red}$ yielding $H_2O_2$.

Next, we tested the photocatalytic reduction of FMN and its aerobic, $H_2O_2$-forming reoxidation to promote r*Aae*UPO-catalysed hydroxylation. Experiments in the absence of either CND or FMN gave no significant product formation, whereas the whole system produced enantiomerically pure (*R*)-1-phenyl ethanol (98% e.e.) (Fig. 8c). Compared to previously used Au-$TiO_2$, the overall reaction rates were significantly higher: initial rates of 0.16 mM $h^{-1}$ and 0.81 mM $h^{-1}$ for Au-$TiO_2$ and CND, respectively. Hence, even under non-optimized conditions, almost 100,000 turnovers for r*Aae*UPO

and more than 100 for FMN were estimated. Similar results were achieved under the same conditions for the hydroxylation of cyclohexane (Supplementary Fig. 37). It is also worth noting that the overoxidation rate was reduced significantly.

Overall, we have combined photochemical water-oxidation catalysis with peroxygenase catalysis to achieve visible-light-driven, aerobic oxidation of hydrocarbons. Combined with further (enzymatic) reaction steps this method gives access to a broad range of functionalized building blocks starting from simple alkanes. Admittedly, the system reported here falls short in terms of space–time yields to be economical or environmentally benign. Particularly, the low concentrations of the hydrophobic substrates need to be increased and mass balance issues of some volatile reagents will have to be addressed. But the catalytic turnover achieved for the biocatalyst compares well with the state-of-the-art in peroxygenase reactions and surpasses the performance of the established P450 monooxygenases and chemical catalysts (Supplementary Table 5). Further improvements may be expected in the near future from optimized reaction schemes, particularly from more active WOCs.

## Methods

**Materials.** Titanium(IV) oxide and water-$^{18}O$ (97 atom% $^{18}O$) were bought from Sigma-Aldrich and used as received. Gold(III) chloride (64.4% minimum) was bought from Alfa-Aesar. All other chemicals were purchased commercially and used without further treatments.

**Photocatalyst preparation.** Both anatase and rutile Au-$TiO_2$ catalysts were prepared by a deposition–precipitation method according to literature procedures[51]. A detailed description of the syntheses is given in the Supplementary Information. Examples of XRD data and TEM images of Au-$TiO_2$ are shown in Supplementary Table 1 and Supplementary Figs. 1–4.

**Enzyme preparation.** Recombinant expression and purification of the evolved unspecific peroxygenase mutant from *A. aegerita* in *P. pastoris* was performed following a previously described procedure[20]. The chloroperoxidase from *C. inaequalis* (*Ci*VCPO) was recombinantly expressed in *E. coli* following a protocol published previously[42]. A detailed description of the production and purification of the enzymes is given in the Supplementary Information.

**Typical protocol for the photoenzymatic hydroxylation of alkanes.** To a transparent glass vial, 5 mg of photocatalyst was added and suspended in 900 µl of NaPi buffer under sonication for 5 min in an ultrasonication bath. From stock solutions, 350 nM of r*Aae*APO and 15 mM of ethyl benzene (final concentrations) were added and the volume of the suspension was adjusted to 1 ml with NaPi buffer. The reaction vial was irradiated by visible light at 30 °C under gentle stirring in a homemade setup (Supplementary Fig. 8) equipped with a white light bulb (Philips 7748XHP 150 W, Supplementary Fig. 9). The distance between the reaction vial and bulb was 3.6 cm. At intervals, aliquots were withdrawn, extracted with ethyl acetate, dried over $MgSO_4$ and analysed by (chiral) gas chromatography. Details of gas chromatograph and temperature profiles are shown in Supplementary Table 4 and Supplementary Figs. 19–27.

For detailed experimental procedures of chemoenzymatic halogenation of phenols and the multi-enzyme cascade reactions, see Supplementary Methods.

**Data availability.** All data are available from the corresponding author upon reasonable request.

Received: 3 May 2017; Accepted: 26 September 2017;
Published online: 20 November 2017

## References

1. Kille, S., Zilly, F. E., Acevedo, J. P. & Reetz, M. T. Regio- and stereoselectivity of P450-catalysed hydroxylation of steroids controlled by laboratory evolution. *Nat. Chem.* **3**, 738–743 (2011).
2. Kudrik, E. V. et al. An N-bridged high-valent diiron-oxo species on a porphyrin platform that can oxidize methane. *Nat. Chem.* **4**, 1024–1029 (2012).
3. Kamata, K., Yonehara, K., Nakagawa, Y., Uehara, K. & Mizuno, N. Efficient stereo- and regioselective hydroxylation of alkanes catalysed by a bulky polyoxometalate. *Nat. Chem.* **2**, 478–483 (2010).
4. Wang, Y., Lan, D., Durrani, R. & Hollmann, F. Peroxygenases en route to becoming dream catalysts. What are the opportunities and challenges? *Curr. Opin. Chem. Biol.* **37**, 1–9 (2017).
5. Ullrich, R., Nüske, J., Scheibner, K., Spantzel, J. & Hofrichter, M. Novel haloperoxidase from the agaric basidiomycete *Agrocybe aegerita* oxidizes aryl alcohols and aldehydes. *Appl. Environ. Microbiol.* **70**, 4575–4581 (2004).
6. Grobe, G. et al. High-yield production of aromatic peroxygenase by the agaric fungus *Marasmius rotula*. *AMB Express* **1**, 31 (2011).
7. Babot, E. D., del Río, J. C., Kalum, L., Martínez, A. T. & Gutiérrez, A. Oxyfunctionalization of aliphatic compounds by a recombinant peroxygenase from *Coprinopsis cinerea*. *Biotechnol. Bioeng.* **110**, 2323–2332 (2013).
8. van Rantwijk, F. & Sheldon, R. A. Selective oxygen transfer catalysed by heme peroxidases: synthetic and mechanistic aspects. *Curr. Opin. Biotechnol.* **11**, 554–564 (2000).
9. Piontek, K. et al. Structural basis of substrate conversion in a new aromatic peroxygenase: P450 functionality with benefits. *J. Biol. Chem.* **288**, 34767–34776 (2013).
10. Molina-Espeja, P. et al. Directed evolution of unspecific peroxygenase from *Agrocybe aegerita*. *Appl. Environ. Microbiol.* **80**, 3496–3507 (2014).
11. Bornscheuer, U. T. et al. Engineering the third wave of biocatalysis. *Nature* **485**, 185–194 (2012).
12. Roiban, G. D., Agudo, R. & Reetz, M. T. Cytochrome P450 catalyzed oxidative hydroxylation of achiral organic compounds with simultaneous creation of two chirality centers in a single C–H activation step. *Angew. Chem. Int. Ed.* **53**, 8659–8663 (2014).
13. Joo, H., Lin, Z. L. & Arnold, F. H. Laboratory evolution of peroxide-mediated cytochrome P450 hydroxylation. *Nature* **399**, 670–673 (1999).
14. Holtmann, D. & Hollmann, F. The oxygen dilemma: a severe challenge for the application of monooxygenases? *ChemBioChem* **17**, 1391–1398 (2016).
15. Trost, B. M. The atom economy: a search for synthetic efficiency. *Science* **254**, 1471–1477 (1991).
16. Ni, Y. et al. Peroxygenase-catalyzed oxyfunctionalization reactions promoted by the complete oxidation of methanol. *Angew. Chem. Int. Ed.* **55**, 798–801 (2016).
17. Krieg, T., Huttmann, S., Mangold, K.-M., Schrader, J. & Holtmann, D. Gas diffusion electrode as novel reaction system for an electro-enzymatic process with chloroperoxidase. *Green Chem.* **13**, 2686–2689 (2011).
18. Kofuji, Y. et al. Graphitic carbon nitride doped with biphenyl diimide: efficient photocatalyst for hydrogen peroxide production from water and molecular oxygen by sunlight. *ACS Catal.* **6**, 7021–7029 (2016).
19. Hirakawa, H. et al. Au nanoparticles supported on $BiVO_4$: effective inorganic photocatalysts for $H_2O_2$ production from water and $O_2$ under visible light. *ACS Catal.* **6**, 4976–4982 (2016).
20. Molina-Espeja, P., Ma, S., Mate, D. M., Ludwig, R. & Alcalde, M. Tandem-yeast expression system for engineering and producing unspecific peroxygenase. *Enz. Microb. Technol.* **73–74**, 29–33 (2015).
21. Mifsud, M. et al. Photobiocatalytic chemistry of oxidoreductases using water as the electron donor. *Nat. Commun.* **5**, 3145 (2014).
22. Churakova, E. et al. Specific photobiocatalytic oxyfunctionalization reactions. *Angew. Chem. Int. Ed.* **50**, 10716–10719 (2011).
23. Diesen, V. & Jonsson, M. Formation of $H_2O_2$ in $TiO_2$ photocatalysis of oxygenated and deoxygenated aqueous systems: a probe for photocatalytically produced hydroxyl radicals. *J. Phys. Chem. C* **118**, 10083–10087 (2014).
24. Teranishi, M., Hoshino, R., Naya, S.-I. & Tada, H. Gold-nanoparticle-loaded carbonate-modified titanium(IV) oxide surface: visible-light-driven formation of hydrogen peroxide from oxygen. *Angew. Chem. Int. Ed.* **55**, 12773–12777 (2016).
25. Li, X. Z., Chen, C. C. & Zhao, J. C. Mechanism of photodecomposition of $H_2O_2$ on $TiO_2$ surfaces under visible light irradiation. *Langmuir* **17**, 4118–4122 (2001).
26. Dvoranová, D., Barbieriková, Z. & Brezová, V. Radical intermediates in photoinduced reactions on $TiO_2$ (an EPR spin trapping study). *Molecules* **19**, 17279 (2014).
27. Schneider, J. et al. Understanding $TiO_2$ photocatalysis: mechanisms and materials. *Chem. Rev.* **114**, 9919–9986 (2014).
28. Marquez, L. A. & Dunford, H. B. Reaction of compound III of myeloperoxidase with ascorbic acid. *J. Biol. Chem.* **265**, 6074–6078 (1990).
29. Bilski, P., Reszka, K., Bilska, M. & Chignell, C. F. Oxidation of the spin trap 5,5-dimethyl-1-pyrroline *N*-oxide by singlet oxygen in aqueous solution. *J. Am. Chem. Soc.* **118**, 1330–1338 (1996).
30. Hanaor, D. A. H. & Sorrell, C. C. Review of the anatase to rutile phase transformation. *J. Mater. Sci.* **46**, 855–874 (2011).
31. Fitzpatrick, T. B., Amrhein, N. & Macheroux, P. Characterization of YqjM, an old yellow enzyme homolog from *Bacillus subtilis* involved in the oxidative stress response. *J. Biol. Chem.* **278**, 19891–19897 (2003).
32. Hanefeld, U., Gardossi, L. & Magner, E. Understanding enzyme immobilisation. *Chem. Soc. Rev.* **38**, 453–468 (2009).
33. Guo, Q. et al. How far can hydroxyl radicals travel? An electrochemical study based on a DNA mediated electron transfer process. *Chem. Commun.* **47**, 11906–11908 (2011).

34. Peter, S. et al. Enzymatic one-pot conversion of cyclohexane into cyclohexanone: comparison of four fungal peroxygenases. *J. Mol. Catal. B Enzym.* **103**, 47–51 (2014).
35. Kluge, M., Ullrich, R., Scheibner, K. & Hofrichter, M. Stereoselective benzylic hydroxylation of alkylbenzenes and epoxidation of styrene derivatives catalyzed by the peroxygenase of *Agrocybe aegerita*. *Green Chem.* **14**, 440–446 (2012).
36. Peter, S. et al. Selective hydroxylation of alkanes by an extracellular fungal peroxygenase. *FEBS J.* **278**, 3667–3675 (2011).
37. Sehl, T. et al. Two steps in one pot: enzyme cascade for the synthesis of nor(pseudo)ephedrine from inexpensive starting materials. *Angew. Chem. Int. Ed.* **52**, 6772–6775 (2013).
38. Hailes, H. C. et al. Engineering stereoselectivity of ThDP-dependent enzymes. *FEBS J.* **280**, 6374–6394 (2013).
39. Höhne, M., Schätzle, S., Jochens, H., Robins, K. & Bornscheuer, U. T. Rational assignment of key motifs for function guides in silico enzyme identification. *Nat. Chem. Biol.* **6**, 807–813 (2010).
40. Hanson, R. L. et al. Preparation of (*R*)-amines from racemic amines with an (*S*)-amine transaminase from *Bacillus megaterium*. *Adv. Synth. Catal.* **350**, 1367–1375 (2008).
41. Both, P. et al. Whole-cell biocatalysts for stereoselective C—H amination reactions. *Angew. Chem. Int. Ed.* **55**, 1511–1513 (2016).
42. Fernández-Fueyo, E. et al. Chemoenzymatic halogenation of phenols by using the haloperoxidase from *Curvularia inaequalis*. *ChemCatChem* **7**, 4035–4038 (2015).
43. van Schijndel, J., Vollenbroek, E. & Wever, R. The chloroperoxidase from the fungus *Curvularia inaequalis*: a novel vanadium enzyme. *Biochim. Biophys. Acta* **1161**, 249–256 (1993).
44. Frank, A., Seel, C. J., Groll, M. & Gulder, T. Characterization of a cyanobacterial haloperoxidase and evaluation of its biocatalytic halogenation potential. *ChemBioChem* **17**, 2028–2032 (2016).
45. Getrey, L., Krieg, T., Hollmann, F., Schrader, J. & Holtmann, D. Enzymatic halogenation of the phenolic monoterpenes thymol and carvacrol with chloroperoxidase. *Green Chem.* **16**, 1104–1108 (2014).
46. Martin, D. J. et al. Highly efficient photocatalytic $H_2$ evolution from water using visible light and structure-controlled graphitic carbon nitride. *Angew. Chem. Int. Ed.* **53**, 9240–9245 (2014).
47. Zhang, W., Bariotaki, A., Smonou, I. & Hollmann, F. Visible-light-driven photooxidation of alcohols using surface-doped graphitic carbon nitride. *Green Chem.* **19**, 2096–2100 (2017).
48. Liu, J. et al. Carbon nanodot surface modifications initiate highly efficient, stable catalysts for both oxygen evolution and reduction reactions. *Adv. Energ. Mater.* **6**, 1502039 (2016).
49. Martindale, B. C. M., Hutton, G. A. M., Caputo, C. A. & Reisner, E. Solar hydrogen production using carbon quantum dots and a molecular nickel catalyst. *J. Am. Chem. Soc.* **137**, 6018–6025 (2015).
50. Hutton, G. A. M. et al. Carbon dots as versatile photosensitizers for solar-driven catalysis with redox enzymes. *J. Am. Chem. Soc.* **138**, 16722–16730 (2016).
51. Priebe, J. B. et al. Solar hydrogen production by plasmonic Au-$TiO_2$ catalysts: impact of synthesis protocol and $TiO_2$ phase on charge transfer efficiency and $H_2$ evolution rates. *ACS Catal.* **5**, 2137–2148 (2015).


## Acknowledgements

Financial support by the European Research Council (ERC Consolidator grant no. 648026) is gratefully acknowledged. The authors thank B. Norder for XRD, W. H. Evers for TEM and F. Hagen for EPR measurements. The authors also thank S. Schmidt for the preparation of benzaldehyde lyase, M. Pesic for the preparation of YqjM and T. Knaus for the preparation of ω-transaminases. F.G.M. received funding as an ERC Starting Grant Fellow (grant agreement 638271).

## Author contributions

W.Z., E.F.-F., Y.N., M.v.S. and J.G. performed the experimental work and analysed the results; R.R., R.W., F.G.M., D.R. and M.A. provided biocatalysts and participated in the planning and analysis of the experiments; W.Z. and F.H. conceived and designed the experiments. All authors co-wrote the manuscript.

## Competing interests

The authors declare no competing financial interests.

## Additional information

**Supplementary information** is available for this paper at https://doi.org/10.1038/s41929-017-0001-5.

**Reprints and permissions information** is available at www.nature.com/reprints.

**Correspondence and requests for materials** should be addressed to F.H.

**Publisher's note:** Springer Nature remains neutral with regard to jurisdictional claims in published maps and institutional affiliations.